Enhancement of a zwitterionic chitosan derivative on mechanical properties and antibacterial activity of carboxymethyl cellulose-based films

Zhang, Cangheng; Yang, Xiaodeng; Li, Yan; Qiao, Congde; Wang, Shoujuan; Wang, Xiaoju; Xu, Chunlin; Yang, Huan; Li, Tianduo

Published in:
International Journal of Biological Macromolecules

DOI:
10.1016/j.ijbiomac.2020.05.080

Published: 15/09/2020

Document Version
Accepted author manuscript

Enhancement of a zwitterionic chitosan derivative on mechanical properties and antibacterial activity of carboxymethyl cellulose-based films

Cangheng Zhang[a], Xiaodeng Yang[a*], Yan Li[a], Congde Qiao[a], Shoujuan Wang[a], Xiaoju Wang[b], Chunlin Xu[b], Huan Yang[a], Tianduo Li[a]

[a] Shandong Key Laboratory of Molecular Engineering; State Key Laboratory of Biobased Material and Green Papermaking, Qilu University of Technology, Shandong Academy of Sciences, Jinan, 250353, China

[b] Laboratory of Natural Materials and Technology, Johan Gadolin Process Chemistry Center, Abo Akademi University, Porthansgatan 3, 20500 Turku, Finland

* Corresponding author, Email: yangxiaodeng@qlu.edu.cn

Tel./Fax.: +86-531-89631212

Abstract

A type of zwitterionic chitosan derivative, *N*-2-hydroxylpropyl-3-trimethylammonium-*O*-carboxymethyl chitosan (HTCMCh), was synthesized and introduced into carboxymethyl cellulose (CMC)-based films as a film strength enhancer and antibacterial agent. The influencing factors include degree of substitution (DS) and m_{HTCMCh}/m_{CMC}. Their influences on mechanical properties, thermal stability, antibacterial activities, microstructures, transmittance, and wettability of the CMC-based films were studied. It was found that HTCMCh improves the tensile strength (by 9.0–130.9%), Young's modulus (47.8–351.6%), and elongation at break (90.8–280.8%) of CMC/HTCMCh films simultaneously, depending on the DS and mass content of HTCMCh. However, the HTCMCh shows little influence on microstructure and thermal stability of CMC/HTCMCh films. Satisfactorily, CMC/HTCMCh films show strong antibacterial activities against *E. coli* and *S. aureus* and are nontoxic to fibroblast HFF-1 cells. Pork packaging experiments demonstrated that CMC/HTCMCh*10%,0,58*

film could significantly inhibit bacterial growth, indicating that the HTCMCh-doped CMC films could be used as food packaging materials.

Keywords: *N*-2-hydroxylpropyl-3-trimethylammonium-*O*-carboxymethyl chitosan (HTCMCh); carboxymethyl cellulose film; physicochemical properties; cytotoxicity; antibacterial activity

1. Introduction

With increasing concerns of biodegradable food packaging films, research on carboxymethyl cellulose (CMC)-based films has been rapidly developing (Han, 2014). CMC is a kind of anionic water-soluble derivative of cellulose, whose films suffer from inferior mechanical properties, non-antibacterial activity, and poor moisture barrier properties. Therefore, numerous scientific studies have been performed to improve mechanical properties (Lan et al., 2018; Oun & Rhim, 2016; Oun & Rhim, 2015; Son et al., 2015; Wang et al., 2018; Yadav et al., 2013; You et al., 2016), thermal stability (Abdulkhani et al., 2016; Akhtar et al., 2018; Baniasad & Ghorbani, 2016), and antibacterial properties (Abdollahi et al., 2019; Akhtar et al., 2018; Hasheminya et al., 2019a; Hasheminya et al., 2019b; Noshirvani et al., 2017) of CMC-based films by incorporating various fillers such as inorganic nanoparticles (Baniasad & Ghorbani, 2016; Dadfar, 2014; El Sayed et al., 2015; You et al., 2016; Youssef et al., 2016), organic compounds (Abdollahi et al., 2019; Hasheminya et al., 2019a; Martelli et al., 2017), macromolecule-based nanomaterials (Abdulkhani et al., 2016; Ampaiwong et al., 2019; He et al., 2019; Mazhari Mousavi et al., 2017; Oun & Rhim, 2016; Oun & Rhim, 2015; Pahimanolis et al., 2013; Son et al., 2015; Yadav et al., 2013), and macromolecules (Akhtar et al., 2018; Arık Kibar & Us, 2013; Cheng et al., 2008; El Sayed et al., 2015; Hu et al., 2016; Kawasaki et al., 2016; Lan et al., 2018; Mu et al., 2012; Noshirvani et al., 2017; Wang et al., 2018).

Additives of different type, size, and morphology show different capabilities with respect to increasing tensile strength of CMC films, such as, cellulose nanofibril (CNF, 5 *wt*% based on m_{CMC}) isolated from cotton linter pulp and cellulose nanocrystals (CNC, 5 *wt*%) isolated from rice straw, where each increased the tensile strengths of

CMC films by 23% (Oun & Rhim, 2015) and 45.7 %(Oun & Rhim, 2016), respectively. Graphene oxide (GO, 1 *wt*%) and reduced graphene oxide (rGO, 2 *wt*%) increased the tensile strength of CMC films by 67% (Yadav et al., 2013) and 72.52% (Son et al., 2015), respectively. These increases were attributed to their homogeneous dispersions in CMC-based film-forming solutions and the formed hydrogen bonds between the additives and CMC. The formation of hydrogen bonds depends on the surface composition of the nanomaterials, where surface treatment processes have been found to be complicated and cumbersome. In contrast, water-soluble compounds are more convenient in preparing film-forming solutions and are effective mechanical film enhancers. Water-soluble polysaccharides from chickpea hull (CHPS, m_{CHPS}/m_{CMC}=1.0 %, c_{CMC}=2% w/v) increased the tensile strength of CMC-based films by 100.57 %(Akhtar et al., 2018), which was much higher than the four nanocomposites mentioned above. This is due to the water solubility and compatibility of CHPS and CMC, as well as the strong intermolecular interactions between CMC and CHPS macromolecules (Akhtar et al., 2018).

Relative to food packaging applications, antibacterial properties are one of the most desired properties for newly developed materials (de Azeredo, 2013; Sung et al., 2013). CNC, CNF, GO and rGO-doped CMC films do not show antibacterial properties. To endow CMC-based films with antibacterial activities, researchers have added inorganic nanoparticles (e.g. CuO, ZnO, MgO, Ag) or essential oils, such as cinnamon oil, ginger oil (Noshirvani et al., 2017), summer savory essential oil (SSEO) (Abdollahi et al., 2019), and satureja khuzestanica essential oil (SEO) (Hasheminya et al., 2019a) into CMC-based films. These doped CMC films show effective antibacterial activities, and the incorporation of metal oxide nanoparticles (such as CuO, ZnO) can form a synergistic antibacterial effect(Hasheminya et al., 2019b). Unfortunately, essential oils also showed negative impacts on CMC film properties, such as reductions in transparency, tensile strength, and elongation at break, as well as increase in water vapor permeability and surface roughness (Atarés & Chiralt, 2016). Additionally, the essential oils usually lead to emulsification of film-forming solutions due to their

hydrophobicity, and demulsification is a time-consuming and costly process (Atarés & Chiralt, 2016).

Chitosan (Ch) is a natural bioactive polysaccharide with intrinsic antimicrobial activities, which has attracted increasing interest in packaging materials (Hu et al., 2016; van den Broek et al., 2015; Wang et al., 2018). To overcome water-insolubility limitations, chitosan is often modified before utilization. We have synthesized a kind of zwitterionic chitosan derivative, *N*-2-hydroxylpropyl-3-trimethyl ammonium-*O*-carboxymethyl chitosan (HTCMCh), which has good water solubility independent of solvent pH, antibacterial activity, thermal stability, and film-forming properties. The tensile strength of HTCMCh film (9.25 MPa) is 1.22 times that *O*-carboxymethyl chitosan film (7.57 MPa), due to the intermolecular interactions(Liu et al., 2020). The $-\mathrm{N}(\mathrm{CH}_3)_3^+$ group in HTCMCh is linked to three methyl groups and is pH-independent of its interaction with $-\mathrm{COO}^-$ in CMC. To the best of our knowledge, there are no reports using this chitosan derivative used as an additive for CMC-based films.

Herein, the effects of HTCMCh on the properties of CMC-based films were studied. These factors are degree of substitution (DS) and mass content of HTCMCh, and the properties studied include mechanical properties, microstructure, whiteness, transmittance, wettability, and antibacterial activity. The CMC/HTCMCh films show improved mechanical properties and antibacterial activities. To reveal the intermolecular interactions between HTCMCh and CMC, rheological properties of film-forming solutions were studied. Finally, CMC/HTCMCh$_{10\%,0.58}$ films were used to package fresh pork and showed excellent antibacterial activity, which validated the possibilities of using CMC/HTCMCh films as packaging materials.

2. Experimental

2.1 Materials

Sodium carboxymethyl cellulose (CMC, UPS grade) is the same as in our previous work (Wang et al., 2018), and HTCMCh (Schematic diagram 1) was synthesized in our laboratory(Liu et al., 2020) with degrees of substitution of 0.23, 0.46 and 0.58, as

determined by ^{1}H NMR. *Aloe juice* extracted from *Aloe vera* (L.) *Burm. F.* was purchased from Yunnan Evergreen Biological Co., Ltd., China. Glycerol (A.R.) was supplied by Sinopharm Chemical Reagent Co., Ltd., China. All reagents were used as received. Fresh pork was purchased from Jiajiayue Supermarket in University Town in the Changqing District, Ji'nan City, China.

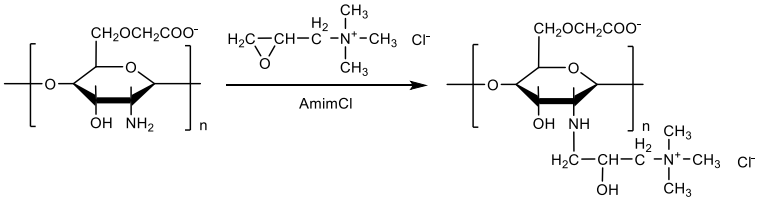

Schematic diagram 1. Molecular structure of HTCMCh, n=0.23, 0.46, and 0.58.

2.2 Preparation of CMC/HTCMCh films

Typically, stock solutions of CMC (4 %, w/v) and HTCMCh (2 %, w/v) are prepared at 80 ºC under magnetic stirring (600 rpm) for 4 hours, and then they are cooled to room temperature and stored at 4 ºC for later use. Twenty-five mL of film-forming solution consisting of 12.5 mL CMC stock solution and calculated amounts of deionized water, HTCMCh stock solution, glycerol, and *aloe juice* were added in turn and magnetically stirred (600 rpm) for 4 h at 60 ºC. The pH values of the film-forming solutions, determined with a Shanghai Thunder Magnetic pH Meter (PHS-25), were in the range of 9.40 to 9.47, depending on m_{HTCMCh}/m_{CMC} The mass ratios of HTCMCh to CMC (m_{HTCMCh}/m_{CMC}) were 0, 1%, 5%, and 10%, and the ratio of glycerol to the total mass of HTCMCh and CMC ($m_{glycerol}/(m_{HTCMCh}+m_{CMC})$) was fixed at 30%.

Twenty-five mL of film-forming solution was poured into a Teflon mold (5.5 cm in diameter and 0.7 cm in height) after degassing. The Teflon mold was transferred into a blast dryer at 40 ºC, and a CMC/HTCMCh film was obtained after the water was evaporated for 48 h. The HTCMCh DS was 0.58, unless specifically noted otherwise. The Fourier transform-infrared spectrum of the CMC/HTCMCh film confirmed the presence of HTCMCh in the film (Fig.S1).

The CMC/HTCMCh film with a m_{HTCMCh}/m_{CMC} of 10% and HTCMCh DS of 0.58 was recorded as CMC/HTCMCh$_{10\%,0.58}$. Other samples designations are similar.

2.3 Characterization of CMC/HTCMCh films

The cross-sectional microstructures were observed on an Evo18 field-emission scanning electron microscope (FESEM) (Carl Zeiss, AG, Germany), which was operated at an accelerating voltage of 3.0 kV. The samples were fractured by liquid nitrogen and sputtered with gold before observation.

The tensile strength (TS) and elongation at break (EB) were measured using the same method as in a previous work (Liu et al., 2020) with slight changes. The tested films were 4.0×1.0 cm strips, and the crosshead speed was 2.0 mm/min. The data was averaged over three different sample strips.

The thicknesses of the CMC/HTCMCh films were measured on an electronic digital Vernier caliper (Shenzhen Duliang Precision Machinery Co., Ltd.) with an accuracy of 0.001 mm. During the measurement, five points were selected for each film, and the values were averaged.

The whiteness and transmittance were tested on a YQ-Z-48B whiteness tester (Hangzhou Qingtong Brocade Automation Technology Co., Ltd., China). An R_{457} whiteboard with whiteness of 84.5 was used in the calibration sample to determine whiteness. A white board with Ry of 84% and a black well as the background was used to measure the transmittance.

Thermogravimetric analysis (TGA) curves were obtained on a thermogravimetric analyzer (TGA, Mettler Toledo, Switzerland) from room temperature to 500 ºC, at a heating rate of 10 ºC/min. A flow velocity of nitrogen of 100 mL/min was used.

The contact angles of the films were measured on a Krüss DSA 100 (Germany) analyzer using the sessile drop method. The angles were read after five seconds of the sessile drop formation.

The antibacterial activity was evaluated by the zone of inhibition method. *Staphylococcus Aureus* (*S. aureus*, ATCC 25923) and *Escherichia Coli* (*E. coli*, ATCC 22922) were used as the bacteria. Culture media consisting of yeast powder (0.5%, w/v), peptone (1.0 %, w/v), NaCl (1.0 %, w/v), and agar powder (1.5 %, w/v) were used, on which the concentrated 100 μL *S. aureus* and *E. coli* samples were spread. Several

sterilized filter paper pieces with diameters of 3.5 mm coupled with same-sized CMC/HTCMCh films with varying m_{HTCMCh}/m_{CMC} were placed on the culture medium. Then the mixed systems were placed in an incubator at 37.5 ºC. The system was recorded for 48 hours.

2.4 Rheological properties of film-forming solutions

The rheological properties of film-forming solutions were measured using a method previously reported(Yang et al., 2020). In short, a DHR-2 rheometer with a parallel plate geometry of 45.0 mm in diameter was used. The gap between the plate and sample stage was set at 1.0 mm. Before dynamic modulus measurements, a linear viscoelastic region was determined at an angular frequency of 1.0 rad/s. The dynamic modulus (storage (G') and loss (G'')) were measured as the angular frequency increased from 0.1 to 100 rad/s. The temperature was fixed at 25 °C. The apparent viscosity was determined within a shear rate of 0.1 to 1000 s^{-1}.

2.5 Cytotoxicity of CMC-HTCMCh mixtures

To test the cytotoxicity of CMC-HTCMCh mixtures, cell viability assays were performed using the 3-(4,5-dimethylthiazol-2-yl)-2,5-diphenyltetrazolium bromide (MTT) (Sigma, USA) assay. Briefly, fibroblast HFF-1 cells were seeded in a 96-well plate (100 μL per well of a suspension containing 1.0×10^5 cells per mL) and incubated for 18 h. Then the cells were treated with CMC/HTCMCh powder for 24 h. The final concentrations of CMC/HTCMCh were 0.5 mg/mL, 1.0 mg/mL, and 2.0 mg/mL, respectively. After treatment, 10 μL of 5 mg/mL MTT were added to each well and the 96-well plate was further incubated at 37 °C for 4 h. Then the cells in each well were rinsed with a phosphate-buffered saline (PBS) buffer and dissolved in 100 μL of dimethyl sulfoxide (DMSO). The absorbances of the samples were measured at 490 nm using a microplate reader (SpectraMax M5; Molecular Devices, USA).

2.6 Application of CMC/HTCMCh$_{10\%,0.58}$ film in fresh pork packaging

Fresh pork was washed with distilled water and cut into small pieces (~9.0 g). Each piece of pork was wrapped in a CMC/HTCMCh$_{10\%,0.58}$ film (11.0 cm in diameter). The pork-loaded packages were transferred into an incubator at 37.5 ºC and observed

every 24 hours.

3. Results and discussion

3.1 Film microstructure

Film properties are directly correlated with the state of the reinforcing agents and their intermolecular interactions. To interpret the effects of HTCMCh on microstructures of CMC film, the cross-sectional SEM images of CMC/HTCMCh and neat (control) films were observed. The control cross-section shows a compact, homogeneous, and smooth surface (Fig. 1A). The addition of HTCMCh shows almost no effect on the cross-sectional morphologies of CMC/HTCMCh$_{10\%,0.23}$ and CMC/HTCMCh$_{10\%,0.46}$ films (Figs. 1B and C) except for occasional flaws, which is different from that of chitosan/cellulose films (Stefanescu et al., 2012). The lack of change is attributed to the water solubility and homogeneity of HTCMCh and CMC (Feng et al., 2018). With increasing DS of HTCMCh, the cross-section of the CMC/HTCMCh$_{10\%,0.58}$ film becomes rough with only occasional flaws but is still continuous (Fig. 1D). At a fixed HTCMCh DS (DS=0.58), the variation in $m_{\mathrm{HTCMCh}}/m_{\mathrm{CMC}}$ shows only small effects on the cross-sectional morphology of CMC/HTCMCh films (Figs. 1E and F). These results suggest good compatibility between HTCMCh and CMC, which might enable films with good gas and water vapor permeabilities (Soni et al., 2016). The effects of water-soluble HTCMCh on CMC film morphologies is different from those of water insoluble chitin nanofibers(Hu et al., 2016). Chitin nanofibers aggregate into microfibers and lead to rough CMC film surfaces with observable voids.

At fixed $m_{\mathrm{HTCMCh}}/m_{\mathrm{CMC}}$ (10%) and HTCMCh DS (0.23), a small amount of $-N(CH_3)_3^+$ can shield the electrostatic repulsion between $-COO^-$ groups, facilitating the ordered arrangement of the two macromolecules. As the HTCMCh DS increases to 0.58, a relatively large amount of $-N(CH_3)_3^+$ interacts with the $-COO^-$ groups, and, there are electrostatic repulsions between HTCMCh and CMC molecules among the $-COO^-$ groups. These two opposite interactions induce CMC aggregation, resulting in

rough cross-sectional surfaces (Wang et al., 2018). The studied HTCMCh contents show relative weak effects on the cross-sectional morphologies of CMC/HTCMCh films.

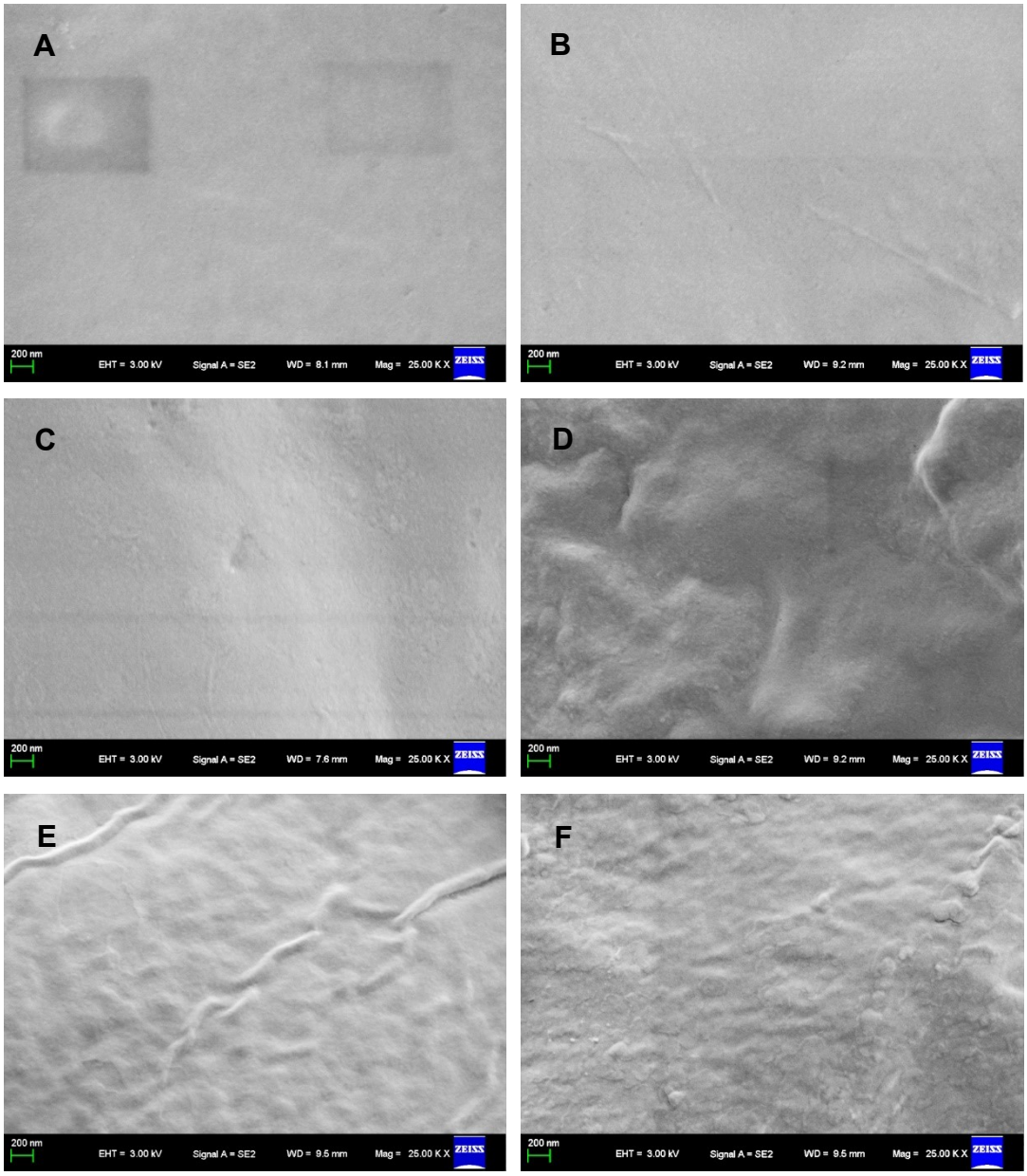

Fig. 1 SEM images of CMC films (A), CMC/HTCMCh$_{10\%}$ films with HTCMCh DSs of 0.23 (B), 0.46 (C) and 0.58 (D), and CMC/HTCMCh$_{0.58}$ films with $m_{\mathrm{HTCMCh}}/m_{\mathrm{CMC}}$ of 5 % (E) and 1% (F), respectively.

3.2 Thickness, whiteness, transmittance, and wettability of films

The thicknesses of the CMC/HTCMCh films are listed in Table 1, from which we could find that with increasing HTCMCh DS from 0.23 to 0.46 and 0.58, the

thicknesses of the CMC/HTCMCh films gradually decreased from 0.238 ± 0.032 to 0.193 ± 0.008, and then to 0.149 ± 0.032 mm, when $m_{\mathrm{HTCMCh}}/m_{\mathrm{CMC}}$ was fixed at 10%. Similarly, the film thickness also decreased with increasing $m_{\mathrm{HTCMCh}}/m_{\mathrm{CMC}}$ at a fixed HTCMCh DS.

It is reported that film thickness depends on the natural properties of film-forming materials, the alignment/interaction between these materials, and the concentration of additives (Li et al., 2016; Shah et al., 2015; Sogut & Seydim, 2018). Both CMC and HTCMCh are water-soluble, and there are oppositely charged groups in the two macromolecules. Namely, strong electrostatic interactions between these two macromolecules dominate their alignment (Ortiz et al., 2018). According to previous work (Wang et al., 2018; Yang et al., 2020), a small mass ratio (such as 1%) of HTCMCh in CMC film-forming solution screens the -COO^- groups and induces intermolecular aggregation of CMC. At a large mass ratio (such as 10%) of HTCMCh, the intermolecular electrostatic interactions, as well as hydrogen bonding, induce tight crosslinking of the two macromolecules. Therefore, the thicknesses of the CMC/HTCMCh films decrease with increasing $m_{\mathrm{HTCMCh}}/m_{CMC}$. As the DS of $\mathrm{HTCMCh}_{10\%}$ decreases, the intermolecular electrostatic interactions are weakened, inducing increased film thickness.

Table 1 Thickness (Th), contact angle (θ), whiteness (W) and transmittance (Tr) of the CMC/HTCMCh films.

Films	Th (mm)	θ (º)	W (%)	Tr (%)
CMC	0.135±0.002	46.2±0.50	38.23±0.19	93.80±0.02
$\mathrm{CMC/HTCMCh}_{10\%,0.23}$	0.238±0.032	42.2±0.45	38.20±0.08	92.07±0.12
$\mathrm{CMC/HTCMCh}_{10\%,0.46}$	0.193±0.008	55.2±0.52	39.33±0.26	91.53±0.09
$\mathrm{CMC/HTCMCh}_{10\%,0.58}$	0.149±0.032	70.6±0.61	37.83±0.05	93.53±0.17
$\mathrm{CMC/HTCMCh}_{5\%,0.58}$	0.205±0.027	77.6±0.60	37.63±0.05	93.77±0.05
$\mathrm{CMC/HTCMCh}_{1\%,0.58}$	0.170±0.010	40.1±0.31	37.97±0.19	93.33±0.09

The whiteness and transmittance of the control CMC film are 38.23 ± 0.19 and

93.80 ± 0.02 %, respectively. The addition of HTCMCh shows almost no influence on the whiteness and transparency of the CMC-based films (Table 1), which is confirmed by the optical appearance (Fig. S2). This means there is good compatibility of the two biomacromolecules.

The intermolecular interaction and arrangement of the macromolecules in the films also affect the surface properties, including wettability and water vapor permeability. The contact angles of the films are listed in Table 1. The contact angles of CMC/HTCMCh$_{5\%,0.58}$ and CMC/HTCMCh$_{10\%,0.58}$ films are 50% higher than the control values, due to the enrichment of $-CH_3$ in $-N(CH_3)_3^+$ on the film surfaces. However, for CMC/HTCMCh$_{10\%,0.23}$ and CMC/HTCMCh$_{1\%,0.58}$ films, the contact angles decrease. This was ascribed to the different intermolecular interactions as the thickness changes. These results are consistent with those obtained in Fig. 1 (current work), *N*-(2-hydroxyl)-propyl-3-trimethylammonium chitosan(HTCC)/CMC films (Wang et al., 2018), and tea polyphenol/hydroxypropyl starch films(Feng et al., 2018).

3.3 Mechanical properties of films

The tensile strength (TS) and elongation at break (EB) of the CMC and CMC/HTCMCh films are shown in Fig. 2. The tensile strength and elongation at break of the neat CMC film are 3.43 MPa and 33.56%, respectively. The mechanical properties of CMC films are affected by several factors, such as resources, molecular mass and molecular mass distribution of CMC, and film-forming conditions (He et al., 2019; Liu et al., 2020; Oun & Rhim, 2019; Wang et al., 2018). Compared with the tensile strength of the neat CMC film, the tensile strengths of CMC/HTCMCh films increase with both HTCMCh DS and its concentration in the films. The tensile strength of the CMC/HTCMCh$_{10\%,0,58}$ film increases by a maximum value of 130.9%, while that of CMC/HTCMCh$_{1\%,0,58}$ film increases by a minimum value of only 9.0%. The maximum increase in Young's modulus (E) is 351.6% (CMC/HTCMCh$_{10\%,0.58}$) and the minimum value is 47.8 % (CMC/HTCMCh$_{1\%,0.58}$). More interestingly and importantly, the EB values of CMC/HTCMCh films also increase after the addition of HTCMCh. The maximum increase of EB is 280.8% (CMC/HTCMCh$_{5\%,0.58}$), followed by a 219.6%

increase (CMC/HTCMCh$_{10\%,0.23}$), and a minimum increase of is 90.8% (CMC/HTCMCh$_{1\%,0.58}$ film).

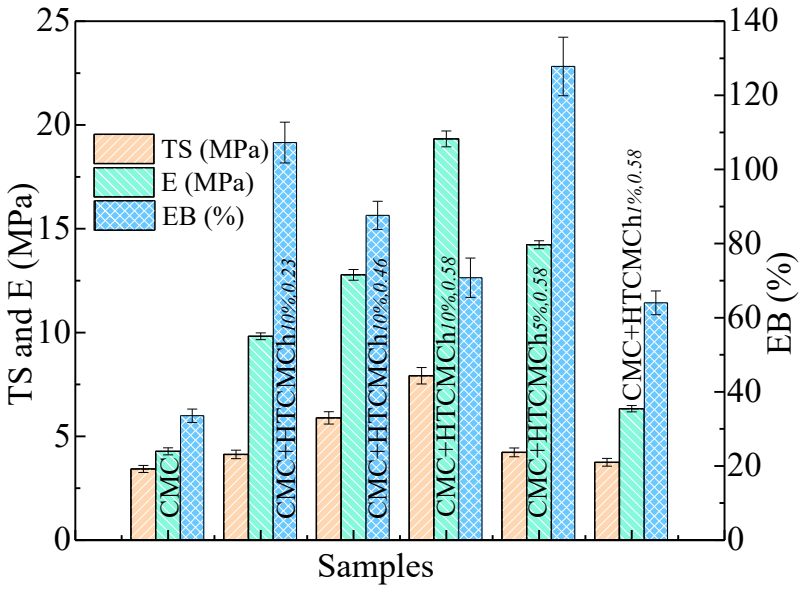

Fig. 2 Tensile strength (TS), elongation at break (EB), and Young's modulus (E) of CMC and CMC/HTCMCh films with different HTCMCh DS and content.

The mechanical properties of complex films are affected by intrinsic characteristics of additive, intermolecular interactions, compatibility of the two macromolecules, and the formed microstructures (Vedadghavami et al., 2017; Yin et al., 2018). Commonly, the additives interact with film-forming substrates through hydrogen bonds, thereby enhancing the tensile strength of the film (Kim et al., 2019). The increase in sliding possibility of polymer chains during deformation results in increased elongation at break (Abdollahi et al., 2019). Commonly, hydrogen bonds between additives and film-forming substrates restrict their relative sliding possibility, resulting in decreased elongation at break. In the current work, the tensile strength, Young's modulus, and elongation at break of CMC-based films increase with the addition of HTCMCh. According to previous reports (Liu et al., 2020; Wang et al., 2018), the increase in tensile strength, elongation at break, and Young's modulus can be attributed to the biocompatibility, strong electrostatic interactions between HTCMCh and CMC, and hydrogen bonding. Similar results were obtained from

pectin/CMC/Ca^{2+} films (Šešlija et al., 2018), PVA/CNC films (Kim et al., 2019), and CNC/lignin films (Zhang et al., 2019).

3.4 Thermal stability of films

TGA curves (Fig.3) show two notable weight losses at ca. 110 ºC (about 16 *wt*%) and 280 ºC (about 50 *wt*%), respectively, for pure CMC and CMC/HTCMCh$_{10\%,0.58}$ films. However, DSC curves show three endothermic peaks. According to literature, the three endothermic peaks correspond to water evaporation, degradation of volatile substances, and degradation of the saccharide skeleton from low to high temperature (Noshirvani et al., 2017; Silva-Pereira et al., 2015), respectively. It should be noted that the decomposition temperature of the CMC/HTCMCh film is the same as that of the CMC film. Commonly, the strong bonds formed between CMC and additives (including inorganic nanoparticles, essential oils, and macromolecules), as well as the rearrangement of the polymer matrix, increase the film's thermal stability (Baniasad & Ghorbani, 2016; Noshirvani et al., 2017). It has also been reported that thermal stability can be impaired due to the disruption of intra- and intermolecular hydrogen bonds, formation of discontinuous structures of the additives, and increased steric hindrance(Tan et al., 2018; Wang et al., 2018). Combined with the FTIR results (Fig. S1), mechanical properties, and cross-sectional microstructures, the thermal stabilities of CMC/HTCMCh films are affected by the disruption of the intra- and intermolecular hydrogen bonds, re-formation of intermolecular interactions, and sterically-hindered structures synergistically.

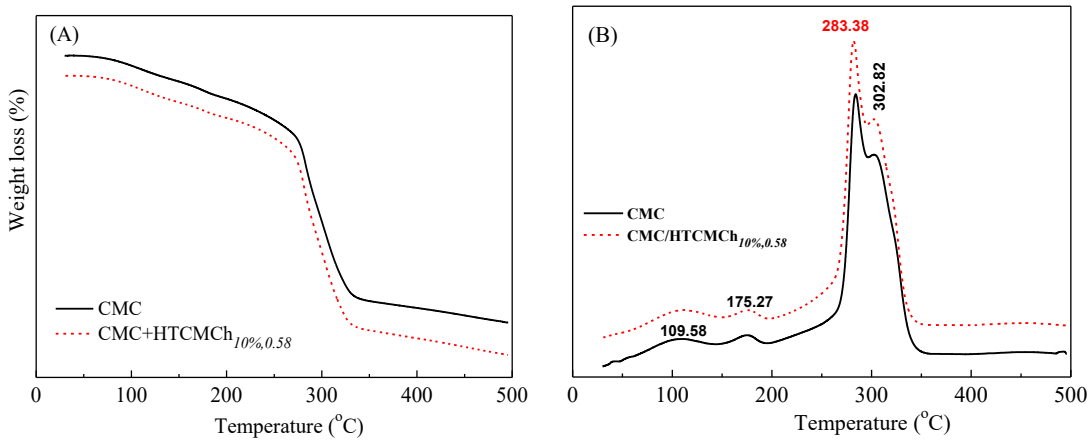

Fig.3 TGA (A) and DSC (B) curves of CMC and CMC/HTCMCh$_{10\%,0.58}$ films.

Results of dynamic mechanical analysis (Fig.S3) show that the glass transition temperature (T_g) of CMC/HTCMCh$_{10\%,0.58}$ is 90.2 °C, which is an increase of 33.7 °C compared to the neat CMC film (56.5 °C). The T_g shifts to higher temperature, due to the presence of intermolecular interactions between HTCMCh and CMC and restricted movement between the two molecules (Ortiz et al., 2018).

3.5 Rheological properties of film-forming solutions

The properties of CMC-based films are related to intermolecular interactions between CMC and additives and their arrangement, which can be reflected through rheological properties of film-forming solutions. All CMC-based film-forming solutions show Newtonian motion plateaus at low shear rates (< 0.4 1/s) and shear thinning behavior at high shear rates (> 0.4 1/s) (Figs. 4A and C). This is ascribed to the intermolecular interactions between CMC and HTCMCh and the formation of the 3D matrix. At high shear rates, the 3D matrix is destroyed, resulting in decreased viscosity. At a fixed m_{HTCMCh}/m_{CMC} (10%), the apparent viscosity is increased by 19.32% (DS: 0.46) and 29.38% (DS: 0.58) with increasing HTCMCh DS. The apparent viscosity of CMC-HTCMCh$_{10\%,0.23}$ solution is approximately equal to that of neat CMC solution. It was shown that the apparent viscosity increased by 10.92 (1%), 25.50 (5%) and 29.38% (10%) with increasing $m_{HTCMCh,0.58}/m_{CMC}$. This is attributed to the intermolecular electrostatic interactions, the hydrogen bonds between HTCMCh and CMC molecules, the variation of predominated intermolecular interactions, and the formation of 3D network structures (Xiao et al., 2015). With the increase of HTCMCh DS at a fixed content, the joint points of electrostatic interaction with $-COO^-$ groups in CMC molecules, as well as hydrogen bonds increased, which resulted in complex structures of the CMC/HTCMCh 3D matrix. As a result, the apparent viscosity of the film-forming solutions increases. The intermolecular interactions also result in viscoelasticity increases (Figs. 4B and D). The storage moduli increase by 7.87% (HTCMCh$_{10\%,0.23}$), 24.78% (HTCMCh$_{10\%,0.46}$), 37.90% (HTCMCh$_{10\%,0.58}$), 14.13% (HTCMCh$_{1\%,0.58}$), and 31.36 % (HTCMCh$_{5\%,0.46}$), respectively.

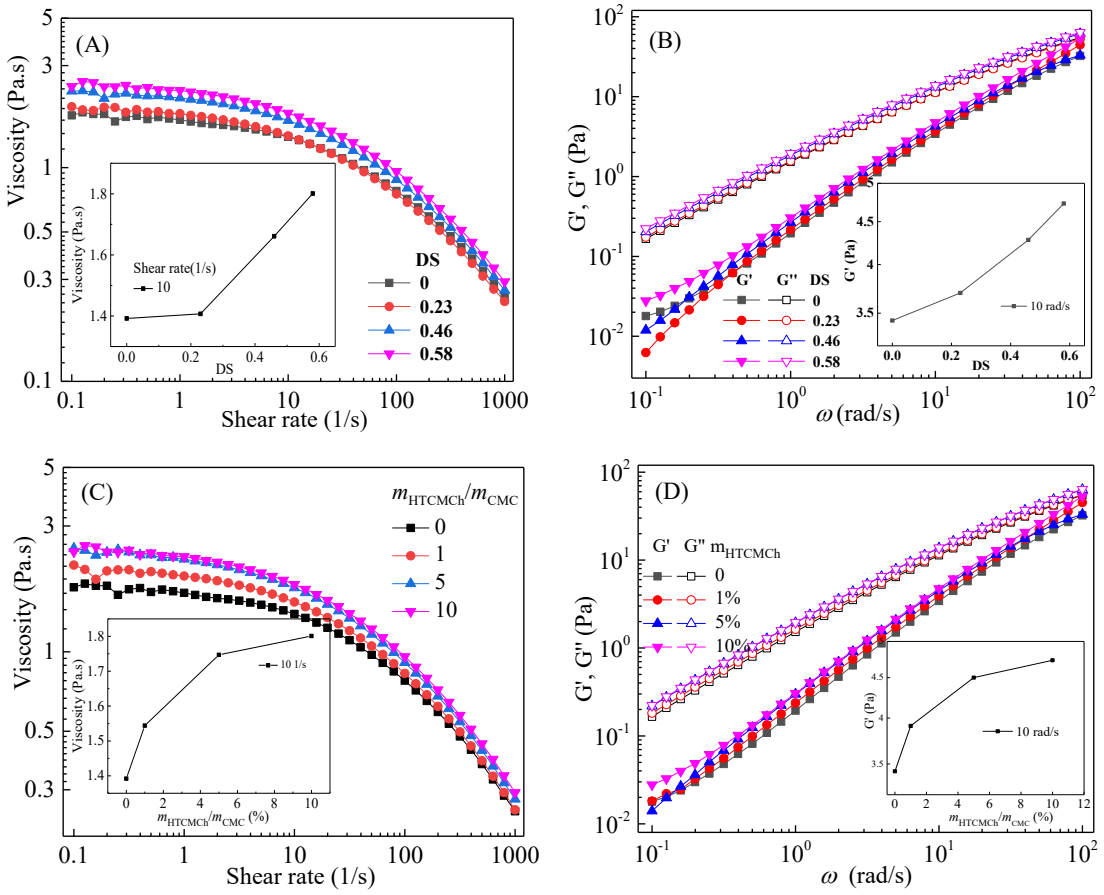

Fig. 4 Apparent viscosity (A and C) and storage moduli (B and D) of CMC/HTCMCh film-forming solutions with different HTCMCh DS and $m_{\mathrm{HTCMCh}}/m_{\mathrm{CMC}}$.

3.6 Antibacterial properties and cytotoxicity of CMC/HTCMCh films

Considering application of CMC/HTCMCh films in food packaging, biocompatibility must be evaluated. The *in vitro* cytotoxicity of the CMC/HTCMCh$_{10\%,0.58}$ film with $c_{HTCMCh_{10\%,0.58}}$ ranging from 0 (control sample) to 2.0 mg/mL was tested by MTT assay. Fig. 5(A) shows that all the CMC/HTCMCh$_{10\%,0.58}$ samples have non-cytotoxicity, which is also HTCMCh$_{10\%,0.58}$ concentration independent. This result is consistent with those reported previously (Guo et al., 2013; Kollar et al., 2011; Sun et al., 2019). Koolar et al. reported that CMCh showed non-cytotoxicity within 148 h (Kollar et al., 2011). Guo et al. revealed that a *N*-trimethyl chitosan coating does not induce additional toxicity at moderate concentrations (Guo et al., 2013). Sun et al. confirmed non-cytotoxicity of *N,O*-CMCh and its derivatives containing thiourea salt on L929 cells(Sun et al., 2019). Therefore,

it can be determined that CMC/HTCMCh films can be safely used as food packaging materials.

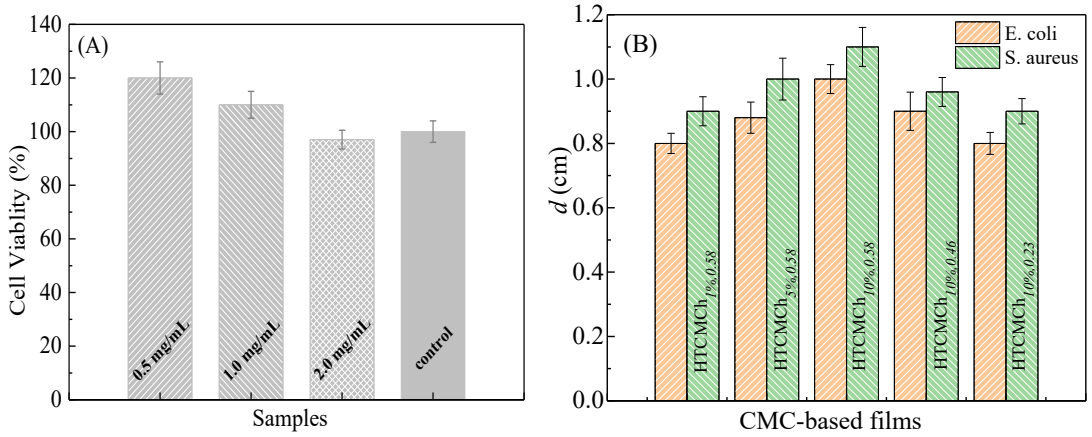

Fig. 5 *In vitro* cytotoxicity (A) and antibacterial properties (B) of CMC/HTCMCh films.

The antibacterial activities of CMC/HTCMCh films with three DSs and three mass ratios against both *E. coli* and *S. aureus* are listed in Fig.5(B). It can be observed that all films show notable antibacterial activities against *E. coli* and *S. aureus*. As it is known that CMC has no antibacterial activities against both *E. coli* and *S. aureus* (Hu et al., 2016), the antibacterial activities of CMC/HTCMCh films are due to the addition of HTCMCh. This result is consistent with those reported by Dehnad et al. (Dehnad et al., 2014) and Park et al.(Park et al., 2010). Dehnad et al.(Dehnad et al., 2014) revealed that chitosan-nanocellulose nanocomposites restrained the growth of *E. coli* and *S. aureus* at a chitosan concentration of 1 *wt*%. The electrostatic interactions between positively charged chitosan or chitosan derivatives and negatively charged bacterial cell membranes play a key role in their antibacterial activity, as electrostatic interactions damage bacterial cell membranes, and kill bacteria (Zheng et al., 2019). Fig. 5(B) shows that the inhibitor zone diameters for *S. aureus* are larger than those for *E. coli*, suggesting that the CMC/HTCMCh films are more effective against *S. aureus*, which has been shown to be susceptible to antibiotics (Azizi et al., 2013; Hu et al., 2016).

3.7 Fresh pork packaging

To test the preservative effects of CMC/HTCMCh$_{10\%,0.58}$ film in food packaging, fresh and clean pork (ca. 9 g) were wrapped with CMC/HTCMCh$_{10\%,0.58}$ films and

stored at 37.5 ºC, while a pure CMC film was used as a control (Fig. 6). The pork surfaces were recorded every 24 h. After 48 h, bacterial growth was observed on the surface of the pork wrapped with CMC film (Fig. 6(A3)). In contrast, the pork surface wrapped with CMC/HTCMCh$_{10\%.0.58}$ film showed no obvious changes, except for slight shrinkage (Fig.6(B3)). According to Wang et al. (Wang et al., 2019), the shrink is caused by water evaporation. After 72 h, obvious bacterial growth was observed on the pork surface wrapped in CMC/HTCMCh$_{10\%.0.58}$ film. These results show that CMC/HTCMCh$_{10\%.0.58}$ film can significantly inhibit bacterial growth. Detailed studies on CMC/HTCMCh film utilization in food packaging are under investigation.

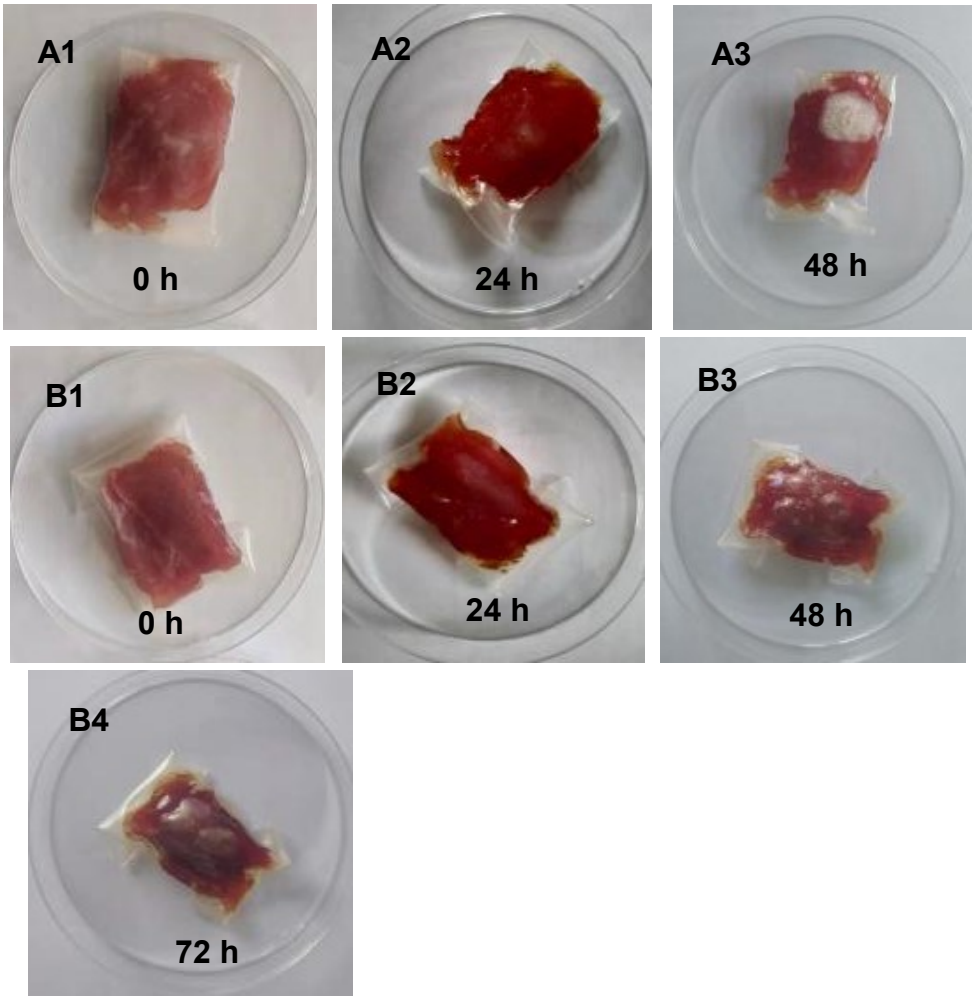

Fig. 6 Photographs of pork-packaged with CMC (A) and CMC/HTCMCh$_{10\%,0.58}$ (B) films.

Conclusions

Rheological properties have illustrated strong intermolecular interactions between

anionic CMC and zwitterionic HTCMCh, inducing the formation of CMC/HTCMCh films with smooth, homogeneous, and connected cross-sectional morphologies. The intermolecular interactions change with variations in HTCMCh content and DS. Interestingly, the addition of HTCMCh increases the tensile strength, Young's modulus, and elongation at break of CMC/HTCMCh films simultaneously. The incremental increases in tensile strength and Young's modulus depend on the HTCMCh DS and mass ratio with CMC. The maximum incremental increase in tensile strength and Young's modulus are 130.9% and 351.6% for the CMC/HTCMCh$_{10\%,0.58}$ film. The maximum incremental increase of elongation at break, obtained for the CMC/HTCMCh$_{5\%,0.58}$ film, is 280.8%. The HTCMCh shows almost no effect on the transmittance and thermal stability of the CMC/HTCMCh films.

HTCMCh is non-cytotoxic and provides the CMC/HTCMCh films with significantly positive antibacterial activities against *E. coli* and *S. aureus*. The CMC/HTCMCh$_{10\%,0.58}$ film can delay the growth of bacteria on packaged fresh pork surface by 48 hours, indicating its potential utility in food packaging.

Acknowledgement

The authors acknowledge the financial support from Program for Scientific Research Innovation Team in Colleges and Universities of Shandong Province, International cooperation Program (QLUTGJHZ2018002), and State Key Laboratory of Biobased Material and Green Papermaking (ZZ20190117), Qilu University of Technology, Shandong Academy of Sciences.

Conflicts of Interest: The authors declare no conflict of interest.

References

Abdollahi, M., Damirchi, S., Shafafi, M., Rezaei, M., Ariaii, P. 2019. Carboxymethyl cellulose-agar biocomposite film activated with summer savory essential oil as an antimicrobial agent. *International Journal of Biological Macromolecules*, **126**, 561-568.

Abdulkhani, A., Daliri Sousefi, M., Ashori, A., Ebrahimi, G. 2016. Preparation and characterization of sodium carboxymethyl cellulose/silk fibroin/graphene oxide nanocomposite films. *Polymer Testing*, **52**, 218-224.

Akhtar, H.M.S., Riaz, A., Hamed, Y.S., Abdin, M., Chen, G., Wan, P., Zeng, X. 2018. Production and characterization of CMC-based antioxidant and antimicrobial films enriched with chickpea hull polysaccharides. *International Journal of Biological Macromolecules*, **118**, 469-477.

Ampaiwong, J., Rattanawaleedirojn, P., Saengkiettiyut, K., Rodthongkum, N., Potiyaraj, P., Soatthiyanon, N. 2019. Reduced Graphene Oxide/Carboxymethyl Cellulose Nanocomposites: Novel Conductive Films. *Journal of Nanoscience and Nanotechnology*, **19**(6), 3544-3550.

Arık Kibar, E.A., Us, F. 2013. Thermal, mechanical and water adsorption properties of corn starch–carboxymethylcellulose/methylcellulose biodegradable films. *Journal of Food Engineering*, **114**(1), 123-131.

Atarés, L., Chiralt, A. 2016. Essential oils as additives in biodegradable films and coatings for active food packaging. *Trends in Food Science & Technology*, **48**, 51-62.

Azizi, S., Ahmad, M., Mahdavi, M., Abdolmohammadi, S. 2013. Preparation, Characterization, and Antimicrobial Activities of ZnO Nanoparticles/Cellulose Nanocrystal Nanocomposites. *BioResources*, **8**, 1841-1851.

Baniasad, A., Ghorbani, M. 2016. Thermal stability enhancement of modified carboxymethyl cellulose films using SnO_2 nanoparticles. *International Journal of Biological Macromolecules*, **86**, 901-906.

Cheng, L.H., Abd Karim, A., Seow, C.C. 2008. Characterisation of composite films made of konjac glucomannan (KGM), carboxymethyl cellulose (CMC) and lipid. *Food Chemistry*, **107**(1), 411-418.

Dadfar, S.M.M., Kavoosi, G. 2015. Mechanical and Water Binding Properties of Carboxymethyl Cellulose/Multiwalled Carbon Nanotube Nanocomposites. *Polymer Composites*, **36**, 145-152.

de Azeredo, H.M.C. 2013. Antimicrobial nanostructures in food packaging. *Trends in Food Science & Technology*, **30**(1), 56-69.

Dehnad, D., Mirzaei, H., Emam-Djomeh, Z., Jafari, S.-M., Dadashi, S. 2014. Thermal and antimicrobial properties of chitosan–nanocellulose films for extending shelf life of ground meat. *Carbohydrate Polymers*, **109**, 148-154.

El Sayed, A.M., El-Gamal, S., Morsi, W.M., Mohammed, G. 2015. Effect of PVA and copper oxide nanoparticles on the structural, optical, and electrical properties of carboxymethyl cellulose films. *Journal of Materials Science*, **50**(13), 4717-4728.

Feng, M., Yu, L., Zhu, P., Zhou, X., Liu, H., Yang, Y., Zhou, J., Gao, C., Bao, X., Chen, P. 2018. Development and preparation of active starch films carrying tea polyphenol. *Carbohydrate Polymers*, **196**, 162-167.

Guo, X.X., He, W., Zhang, X.J., Hu, X.M. 2013. Cytotoxicity of Cationic Liposomes Coated by N-Trimethyl Chitosan and Their In Vivo Tumor Angiogenesis Targeting Containing Doxorubicin. *Journal of Applied Polymer Science*, **128**, 21-27.

Han, J.H. 2014. Chapter 9 - Edible Films and Coatings: A Review. in: *Innovations in Food Packaging (Second Edition)*, (Ed.) J.H. Han, Academic Press. San Diego, pp. 213-255.

Hasheminya, S.-M., Mokarram, R.R., Ghanbarzadeh, B., Hamishekar, H., Kafil, H.S., Dehghannya, J. 2019a. Development and characterization of biocomposite films made from kefiran, carboxymethyl cellulose and Satureja Khuzestanica essential oil. *Food Chemistry*, **289**, 443-452.

Hasheminya, S.-M., Mokarram, R.R., Ghanbarzadeh, B., Hamishekar, H., Kafil, H.S., Dehghannya, J. 2019b. Influence of simultaneous application of copper oxide nanoparticles and Satureja Khuzestanica essential oil on properties of kefiran–carboxymethyl cellulose films. *Polymer*

Testing, **73**, 377-388.

He, Y., Fei, X., Li, H. 2019. Carboxymethyl cellulose-based nanocomposites reinforced with montmorillonite and ε-poly-l-lysine for antimicrobial active food packaging. *Journal of Applied Polymer Science*, 137, 48782.

Hu, D., Wang, H., Wang, L. 2016. Physical properties and antibacterial activity of quaternized chitosan/carboxymethyl cellulose blend films. *LWT - Food Science and Technology*, **65**, 398-405.

Kawasaki, T., Nakaji-Hirabayashi, T., Masuyama, K., Fujita, S., Kitano, H. 2016. Complex film of chitosan and carboxymethyl cellulose nanofibers. *Colloids and Surfaces B: Biointerfaces*, **139**, 95-99.

Kim, J.W., Park, H., Lee, G., Jeong, Y.R., Hong, S.Y., Keum, K., Yoon, J., Kim, M.S., Ha, J.S. 2019. Paper-Like, Thin, Foldable, and Self-Healable Electronics Based on PVA/CNC Nanocomposite Film. *Advanced Functional Materials*, **29**(50), 1905968.

Kollar, P., Závalová, V., Hošek, J., Havelka, P., Sopuch, T., Karpíšek, M., Třetinová, D., Suchý, P. 2011. Cytotoxicity and effects on inflammatory response of modified types of cellulose in macrophage-like THP-1 cells. *International Immunopharmacology*, **11**(8), 997-1001.

Lan, W., He, L., Liu, Y. 2018. Preparation and Properties of Sodium Carboxymethyl Cellulose/Sodium Alginate/Chitosan Composite Film. *Coatings*, **8**(8). 291.

Li, M.-C., Wu, Q., Song, K., Cheng, H., Suzuki, S., Lei, T. 2016. Chitin Nanofibers as Reinforcing and Antimicrobial Agents in Carboxymethyl Cellulose Films: Influence of Partial Deacetylation. *ACS Sustainable Chemistry & Engineering*, **4**, 4385-4395.

Liu, Q., Chen, J., Yang, X., Qiao, C., Li, Z., Xu, C., Li, Y., Chai, J. 2020. Synthesis, structure, and properties of N-2-hydroxylpropyl-3-trimethylammonium-O-carboxymethyl chitosan derivatives. *International Journal of Biological Macromolecules*, **144**, 568-577.

Martelli, S.M., Motta, C., Caon, T., Alberton, J., Bellettini, I.C., do Prado, A.C.P., Barreto, P.L.M., Soldi, V. 2017. Edible carboxymethyl cellulose films containing natural antioxidant and surfactants: α-tocopherol stability, in vitro release and film properties. *LWT*, **77**, 21-29.

Mazhari Mousavi, S.M., Afra, E., Tajvidi, M., Bousfield, D.W., Dehghani-Firouzabadi, M. 2017. Cellulose nanofiber/carboxymethyl cellulose blends as an efficient coating to improve the structure and barrier properties of paperboard. *Cellulose*, **24**(7), 3001-3014.

Mu, C., Guo, J., Li, X., Lin, W., Li, D. 2012. Preparation and properties of dialdehyde carboxymethyl cellulose crosslinked gelatin edible films. *Food Hydrocolloids*, **27**(1), 22-29.

Noshirvani, N., Ghanbarzadeh, B., Gardrat, C., Rezaei, M.R., Hashemi, M., Le Coz, C., Coma, V. 2017. Cinnamon and ginger essential oils to improve antifungal, physical and mechanical properties of chitosan-carboxymethyl cellulose films. *Food Hydrocolloids*, **70**, 36-45.

Ortiz, J.A., Matsuhiro, B., Zapata, P.A., Corrales, T., Catalina, F. 2018. Preparation and characterization of maleoylagarose/PNIPAAm graft copolymers and formation of polyelectrolyte complexes with chitosan. *Carbohydrate Polymers*, **182**, 81-91.

Oun, A.A., Rhim, J.-W. 2016. Isolation of cellulose nanocrystals from grain straws and their use for the preparation of carboxymethyl cellulose-based nanocomposite films. *Carbohydrate Polymers*, **150**, 187-200.

Oun, A.A., Rhim, J.-W. 2015. Preparation and characterization of sodium carboxymethyl cellulose/cotton linter cellulose nanofibril composite films. *Carbohydrate Polymers*, **127**,

101-109.

Oun, A.A., Rhim, J.-W. 2019. Preparation of multifunctional carboxymethyl cellulose-based films incorporated with chitin nanocrystal and grapefruit seed extract. *International Journal of Biological Macromolecules*, https:doi.org/10.1016/j.ijbiomac.2019.10.191.

Pahimanolis, N., Salminen, A., Penttilä, P.A., Korhonen, J.T., Johansson, L.-S., Ruokolainen, J., Serimaa, R., Seppälä, J. 2013. Nanofibrillated cellulose/carboxymethyl cellulose composite with improved wet strength. *Cellulose*, **20**(3), 1459-1468.

Park, S.-i., Marsh, K.S., Dawson, P. 2010. Application of chitosan-incorporated LDPE film to sliced fresh red meats for shelf life extension. *Meat Science*, **85**(3), 493-499.

Šešlija, S., Nešić, A., Škorić, M.L., Krušić, M.K., Santagata, G., Malinconico, M. 2018. Pectin/Carboxymethylcellulose Films as a Potential Food Packaging Material. *Macromolecular Symposia*, **378**(1), 1600163.

Shah, U., Gani, A., Ashwar, B., Shah, A., Ahmad, M., Gani, A., Wani, I., Masoodi, F.A., Yildiz, F. 2015. A review of the recent advances in starch as active and nanocomposite packaging films. *Cogent Food & Agriculture*, **1**, 1115640.

Silva-Pereira, M.C., Teixeira, J.A., Pereira-Júnior, V.A., Stefani, R. 2015. Chitosan/corn starch blend films with extract from Brassica oleraceae (red cabbage) as a visual indicator of fish deterioration. *LWT - Food Science and Technology*, **61**(1), 258-262.

Sogut, E., Seydim, A.C. 2018. Development of Chitosan and Polycaprolactone based active bilayer films enhanced with nanocellulose and grape seed extract. *Carbohydrate Polymers*, **195**, 180-188.

Son, Y.-R., Rhee, K.Y., Park, S.-J. 2015. Influence of reduced graphene oxide on mechanical behaviors of sodium carboxymethyl cellulose. *Composites Part B: Engineering*, **83**, 36-42.

Soni, B., Hassan, E.B., Schilling, M.W., Mahmoud, B. 2016. Transparent bionanocomposite films based on chitosan and TEMPO-oxidized cellulose nanofibers with enhanced mechanical and barrier properties. *Carbohydrate Polymers*, **151**, 779-789.

Stefanescu, C., Daly, W.H., Negulescu, I.I. 2012. Biocomposite films prepared from ionic liquid solutions of chitosan and cellulose. *Carbohydrate Polymers*, **87**(1), 435-443.

Sun, X., Zhang, J., Chen, Y., Mi, Y., Tan, W., Li, Q., Dong, F., Guo, Z. 2019. Synthesis, Characterization, and the Antioxidant Activity of Carboxymethyl Chitosan Derivatives Containing Thiourea Salts. *Polymers*, **11**(11), 1810.

Sung, S.-Y., Sin, L.T., Tee, T.-T., Bee, S.-T., Rahmat, A.R., Rahman, W.A.W.A., Tan, A.-C., Vikhraman, M. 2013. Antimicrobial agents for food packaging applications. *Trends in Food Science & Technology*, **33**(2), 110-123.

Tan, W., Li, Q., Dong, F., Zhang, J., Luan, F., Wei, L., Chen, Y., Guo, Z. 2018. Novel cationic chitosan derivative bearing 1,2,3-triazolium and pyridinium: Synthesis, characterization, and antifungal property. *Carbohydrate Polymers*, **182**, 180-187.

van den Broek, L.A.M., Knoop, R.J.I., Kappen, F.H.J., Boeriu, C.G. 2015. Chitosan films and blends for packaging material. *Carbohydrate Polymers*, **116**, 237-242.

Vedadghavami, A., Minooei, F., Mohammadi, M.H., Khetani, S., Rezaei Kolahchi, A., Mashayekhan, S., Sanati-Nezhad, A. 2017. Manufacturing of hydrogel biomaterials with controlled mechanical properties for tissue engineering applications. *Acta Biomaterialia*, **62**, 42-63.

Wang, B., Yang, X., Qiao, C., Li, Y., Li, T., Xu, C. 2018. Effects of chitosan quaternary ammonium

salt on the physicochemical properties of sodium carboxymethyl cellulose-based films. *Carbohydrate Polymers*, **184**, 37-46.

Wang, H., Gong, X., Miao, Y., Guo, X., Liu, C., Fan, Y.-Y., Zhang, J., Niu, B., Li, W. 2019. Preparation and characterization of multilayer films composed of chitosan, sodium alginate and carboxymethyl chitosan-ZnO nanoparticles. *Food Chemistry*, **283**, 397-403.

Xiao, Q., Tong, Q., Zhou, Y., Deng, F. 2015. Rheological properties of pullulan-sodium alginate based solutions during film formation. *Carbohydrate Polymers*, **130**, 49-56.

Yadav, M., Rhee, K.Y., Jung, I.H., Park, S.J. 2013. Eco-friendly synthesis, characterization and properties of a sodium carboxymethyl cellulose/graphene oxide nanocomposite film. *Cellulose*, **20**(2), 687-698.

Yang, X., Wang, B., Qiao, C., Li, Z., Li, Y., Xu, C., Li, T. 2020. Molecular interactions in N-[(2-hydroxyl)-propyl-3-trimethyl ammonium] chitosan chloride-sodium alginate polyelectrolyte complexes. *Food Hydrocolloids*, **100**, 105400.

Yin, M., Lin, X., Ren, T., Li, Z., Ren, X., Huang, T.-S. 2018. Cytocompatible quaternized carboxymethyl chitosan/poly(vinyl alcohol) blend film loaded copper for antibacterial application. *International Journal of Biological Macromolecules*, **120**, 992-998.

You, Y., Zhang, H., Liu, Y., Lei, B. 2016. Transparent sunlight conversion film based on carboxymethyl cellulose and carbon dots. *Carbohydrate Polymers*, **151**, 245-250.

Youssef, A.M., El-Sayed, S.M., El-Sayed, H.S., Salama, H.H., Dufresne, A. 2016. Enhancement of Egyptian soft white cheese shelf life using a novel chitosan/carboxymethyl cellulose/zinc oxide bionanocomposite film. *Carbohydrate Polymers*, **151**, 9-19.

Zhang, Y., Xu, W., Wang, X., Ni, S., Rosqvist, E., Smått, J.-H., Peltonen, J., Hou, Q., Qin, M., Willför, S., Xu, C. 2019. From Biomass to Nanomaterials: A Green Procedure for Preparation of Holistic Bamboo Multifunctional Nanocomposites Based On Formic Acid Rapid Fractionation. *ACS Sustainable Chemistry & Engineering*, **7**(7), 6592-6600.

Zheng, J., Li, Y., Yang, X., Wei, T., Li, T. 2019. Aggregation behavior and reactivity of N-alkyl-N,N-dimethyl-N-(2,3-epoxy propyl) ammonium chloride. *Journal of Dispersion Science and Technology*, 1-11.